Hidden k-Space Magnetoelectric Multipoles in Nonmagnetic Ferroelectrics

Sayantika Bhowal,[1,*] Stephen P. Collins,[2] and Nicola A. Spaldin[1]
[1]Materials Theory, ETH Zurich, Wolfgang-Pauli-Strasse 27, 8093 Zurich, Switzerland
[2]Diamond Light Source Ltd, Diamond House, Harwell Science and Innovation Campus, Didcot, Oxfordshire OX11 0DE, United Kingdom

(Received 23 September 2021; revised 16 December 2021; accepted 22 February 2022; published 18 March 2022)

In condensed matter systems, the electronic degrees of freedom are often entangled to form complex composites, known as hidden orders, which give rise to unusual properties, while escaping detection in conventional experiments. Here we demonstrate the existence of hidden k-space magnetoelectric multipoles in nonmagnetic systems with broken space-inversion symmetry. These k-space magnetoelectric multipoles are reciprocal to the real-space charge dipoles associated with the broken inversion symmetry. Using the prototypical ferroelectric $PbTiO_3$ as an example, we show that their origin is a spin asymmetry in momentum space resulting from the broken space inversion symmetry associated with the ferroelectric polarization. In $PbTiO_3$, the k-space spin asymmetry corresponds to a pure k-space magnetoelectric toroidal moment, which can be detected using magnetic Compton scattering, an established tool for probing magnetism in ferromagnets or ferrimagnets with a net spin polarization, which has not been exploited to date for *nonmagnetic* systems. In particular, the k-space magnetoelectric toroidal moment combined with the spin-orbit interaction manifest in an antisymmetric magnetic Compton profile that can be reversed using an electric field. Our work suggests an experimental route to directly measuring and tuning hidden k-space magnetoelectric multipoles via specially designed magnetic Compton scattering measurements.

DOI: 10.1103/PhysRevLett.128.116402

Spin-orbit interaction (SOI)-induced spin splitting of the electronic energy bands in materials is central to the design of many spintronic devices [1–5]. The presence of the SOI in ferroelectric materials provides additional tunability of the spin texture through electric-field manipulation of the polarization [6,7], motivating recent research in identifying and designing materials for practical applications [8–12]. Here, we show that the spin texture in ferroelectrics (or in general in nonmagnetic systems with broken inversion ($\mathcal{I}$) symmetry) is a consequence of ordered magnetoelectric multipoles (MEMs) in k space. We illustrate the behavior in the prototypical ferroelectric $PbTiO_3$, for which the real-space electric dipole corresponds to a reciprocal-space magnetoelectric toroidal moment. Finally, we show that the k-space MEMs combined with the SOI give rise to a magnetic Compton profile (MCP), which was previously unknown in nonmagnetic systems, and which provides a platform for their direct detection.

In real space, the MEMs, defined by $\vec{r} \otimes \vec{\mu}$, where $\vec{\mu}$ is the magnetization density, break both $\mathcal{I}$ and time-reversal ($\mathcal{T}$) symmetries. As a result, they are well established for describing the linear magnetoelectric response of materials, in which a magnetization is induced by an electric field and vice versa [13–15]. Of particular interest is the toroidal moment, $\vec{t}$ [Fig. 1(a) upper left], which is the antisymmetric irreducible component of the MEM, for example $t_z = x\mu_y - y\mu_x$. In addition to causing an off-diagonal linear magnetoelectric response, the toroidal moment is proposed to be the order parameter of hidden *ferrotoroidic* order [14,16,17], is linked to skyrmions [18] and antiferromagnetic spintronics [19,20], and is even implicated in the pseudogap phase of cuprate superconductors [21–23].

In contrast to the real-space MEMs, the k-space representations of the MEMs, which are defined by $\vec{k} \otimes \vec{\mu}$, break only $\mathcal{I}$ symmetry, while $\mathcal{T}$ symmetry is preserved. This is a result of the nontrivial duality between real and k space [24,25] [Fig. 1(a)]: On inversion, both $\vec{r}$ and $\vec{k}$ change sign, $\vec{r} \xrightarrow{\mathcal{I}} -\vec{r}$ and $\vec{k} \xrightarrow{\mathcal{I}} -\vec{k}$, whereas on time reversal, $\vec{k}$ changes sign but $\vec{r}$ does not, $\vec{k} \xrightarrow{\mathcal{T}} -\vec{k}$, but $\vec{r} \xrightarrow{\mathcal{T}} \vec{r}$. Since $\vec{\mu} \xrightarrow{\mathcal{T}} -\vec{\mu}$, the k-space MEM, which is the product of $\vec{k}$ and $\vec{\mu}$, is time-reversal symmetric and space-inversion antisymmetric. The consequences of this, which we explore throughout the remainder of this Letter are twofold: (i) Any crystal symmetry that does not contain inversion in real space allows a magnetoelectric multipole in k space. (ii) A magnetoelectric multipole in k space has a nonzero

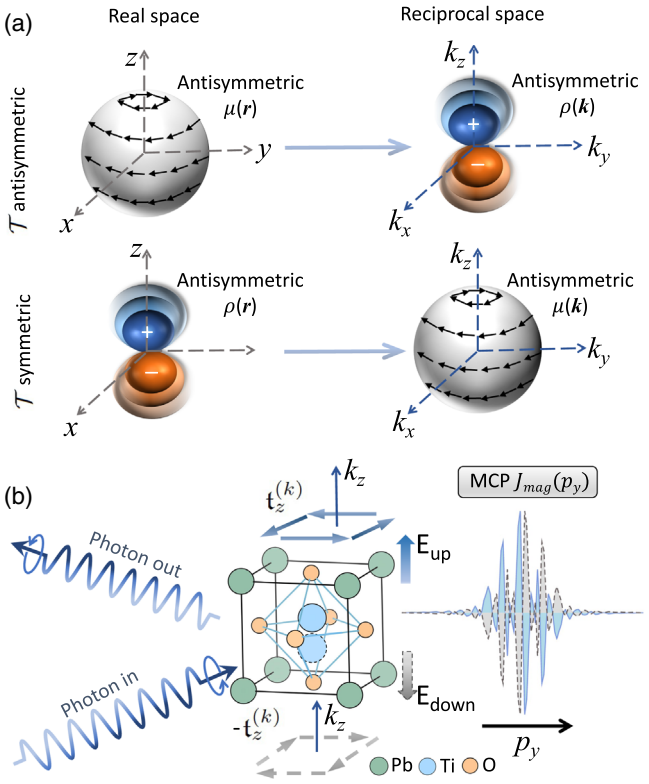

FIG. 1. (a) Transformations (denoted by the big arrows) between real (left) and k-space (right) multipoles in $\mathcal{T}$ antisymmetric (top) and symmetric (bottom) systems with broken $\mathcal{I}$ symmetry. (b) Magnetic Compton scattering with a circularly polarized photon beam in $PbTiO_3$. The solid-outlined Ti-atom position, $\mathbf{t}_z^{(k)}$ spins, and MCP indicate one polarization orientation. With reversed E (dashed outlines), the Ti ion displacement reverses, the toroidal moment $\mathbf{t}_z^{(k)} \rightarrow -\mathbf{t}_z^{(k)}$, and the sign of the MCP reverses.

MCP. As a result, an apparently nonmagnetic electric polarization will cause a magnetic signal in an appropriately designed Compton scattering measurement.

To further illustrate this point we consider the example of $PbTiO_3$, which adopts the tetragonal $P4mm$ structure [26] with C_{4v} point group symmetry. The absence of $\mathcal{I}$ in the C_{4v} symmetry allows for several odd-parity charge multipoles, of which the Q_{10} dipole, z [Fig. 1(a), lower left], which has irreducible representation (IR) A_1^+ in the $PbTiO_3$ structure (Table I), is the lowest order. As expected from the duality discussed above, the corresponding k-space representation $k_x\mu_y - k_y\mu_x$ [see Table I and Fig. 1(a) lower right] is an odd function in $\vec{k}$ and has explicit $\vec{\mu}$ dependence, so it is even under $\mathcal{T}$ as required. Note that $k_x\mu_y - k_y\mu_x = \mathbf{t}_z^{(k)}$ is a toroidal moment in k space; such pure toroidal moments are rare in real space, where they are usually accompanied by magnetoelectric quadrupole moments [14,15,20,25,27].

Recently, Compton scattering [31], an inelastic scattering of x-ray photons by electrons, has been proposed as a possible probe for the direct detection of real-space MEMs [25,32,33]. Based on the duality relations discussed above, a real-space MEM corresponds to an electric dipole (with no magnetization dependence) in reciprocal space, as shown in the top panel of Fig. 1(a). Since Compton scattering measures the electron density in momentum space, the antisymmetric electron density of a k-space electric dipole gives rise to an antisymmetric signal in the *regular* (nonmagnetic) Compton profile [25].

The key result of this work is to extend this argument and show that magnetic Compton scattering, which measures the *spin-dependent* electron momentum distribution [34], can be used to probe the k-space MEMs of a nonmagnetic system. Here, the measured quantity, the MCP $J_{\mathrm{mag}}(p_z)$, is the one-dimensional projection of the spin-polarized electron momentum density along the direction of the scattering vector p_z,

$$J_{\mathrm{mag}}(p_z) = \int\int [\rho^{\uparrow}(\vec{p}) - \rho^{\downarrow}(\vec{p})]dp_x dp_y. \qquad (1)$$

$\rho^{\uparrow}(\vec{p})$ $[\rho^{\downarrow}(\vec{p})]$ is the density of the majority (minority) spin electrons in the momentum space. Since a spin-polarized electron density is typical for systems with net magnetization (i.e., breaks $\mathcal{T}$ symmetry), magnetic Compton

TABLE I. The real space and k-space basis functions of the odd parity charge multipoles (lowest order in k) corresponding to the IR representations of $PbTiO_3$ and GeTe [24,28–30]. The magnetic moment $\vec{\mu}$ includes both orbital and spin contributions.

	Real space		k space	
IR	Multipole	Basis	Multipole	Basis
		$PbTiO_3$ (C_{4v})		
A_1^+	Q_{10}	z	$\mathbf{t}_z^{(k)}$	$k_x\mu_y - k_y\mu_x$
		GeTe (C_{3v})		
A_1^+	Q_{10}	z	$\mathbf{t}_z^{(k)}$	$k_x\mu_y - k_y\mu_x$
E^+	$\{Q_{11}^+, Q_{11}^-\}$	$\{x, y\}$	$\{\mathcal{Q}_{yz}^{(k)}, \mathcal{Q}_{xz}^{(k)}\}$	$\{k_y\mu_z + k_z\mu_y, k_z\mu_x + k_x\mu_z\}$
	$\{Q_{31}^+, Q_{31}^-\}$		$\{\mathbf{t}_x^{(k)}, \mathbf{t}_y^{(k)}\}$	$\{k_y\mu_z - k_z\mu_y, k_z\mu_x - k_x\mu_z\}$
	$\{Q_{32}^+, Q_{32}^-\}$	$\{(x^2 - y^2)z, xyz\}$	$\{\mathcal{Q}_{xy}^{(k)}, \mathcal{Q}_{x^2-y^2}^{(k)}\}$	$\{k_x\mu_y + k_y\mu_x, k_x\mu_x - k_y\mu_y\}$

scattering has to date only been performed in ferro- or ferrimagnetic materials [35–47], where it has been used to extract spin polarizations at Fermi surfaces [44–46] and to separate magnetizations into their spin and orbital [36–38], or localized and itinerant electron contributions [39–43]. As the MCP is a measure of the spin-polarized electron momentum density, however, it is clear that a net magnetization is not required, and that a material with k-space MEMs, and, correspondingly, an antisymmetric k-space magnetization density, will give rise to an antisymmetric MCP in the presence of SOI. This means that a nonzero MCP can occur in a nonmagnetic material provided that the $\mathcal{I}$ symmetry is broken. Since the k-space MEM determines both the magnitude and direction of the antisymmetric MCP, the MCP, in turn, can be used to detect the k-space MEM. We note that an antisymmetric MCP in a nonmagnetic system is consistent with the presence of $\mathcal{T}$ symmetry, which dictates $J_{\mathrm{mag}}(p_z) \xrightarrow{\mathcal{I}} -J_{\mathrm{mag}}(-p_z)$. In contrast, in the centrosymmetric, nonmagnetic case with both $\mathcal{I}$ and $\mathcal{T}$ symmetries, the MCP is zero since $J_{\mathrm{mag}}(p_z) \xrightarrow{\mathcal{I}} J_{\mathrm{mag}}(-p_z)$.

Next, we illustrate the above ideas by explicitly computing the MCP and the odd-parity multipoles for the prototype tetragonal ferroelectric $PbTiO_3$, using first-principles methods based on density functional theory (DFT) as implemented in extended versions [15,48] of the Elk code [49]. The odd-parity charge multipoles are extracted by decomposing the $\mathcal{T}$ symmetric density matrix $\rho_{lm,l'm'}$ into parity-odd tensor moments, where only the odd $l - l'$ terms contribute to the desired multipoles [15]. We choose a ferroelectric for our demonstration because the electric polarization, and in turn the real-space odd-parity multipoles, can be readily switched using an electric field. This in turn allows for switching of the k-space MEMs and the MCP, as illustrated for $PbTiO_3$ in Fig. 1(b). Such an electrical tuning of the MCP is also advantageous over the conventional experiments with magnetic field, as we discuss later.

Our calculated MCP of $PbTiO_3$ [50] is shown in Fig. 2(a). We note first that the computed MCPs are antisymmetric and so satisfy the net moment, $m = \int_{-\infty}^{\infty} J_{\mathrm{mag}}(p_x) dp_x = \int_{-\infty}^{\infty} J_{\mathrm{mag}}(p_y) dp_y = 0$, as required for a nonmagnetic system. The computed MCP is about three orders of magnitude smaller than the corresponding total Compton profile and is about an order of magnitude smaller than the MCP for ferromagnetic Ni [51]. The computed MCPs along p_x and p_y are consistent with the toroidal moment $\mathbf{t}_z^{(k)}$, which indicates the presence of magnetically polarized bands with magnetic orientation along y (x) in the k_x (k_y) direction of momentum space. Note that the signs of the MCPs along p_x and p_y are opposite, directly reflecting the opposite signs of k_x and k_y in $\mathbf{t}_z^{(k)} = k_x \mu_y - k_y \mu_x$. These asymmetries are also reflected in the spin asymmetry in the calculated band structure along the $\pm k_x$ (or $\pm k_y$) directions, shown in Fig. 2(b). The band

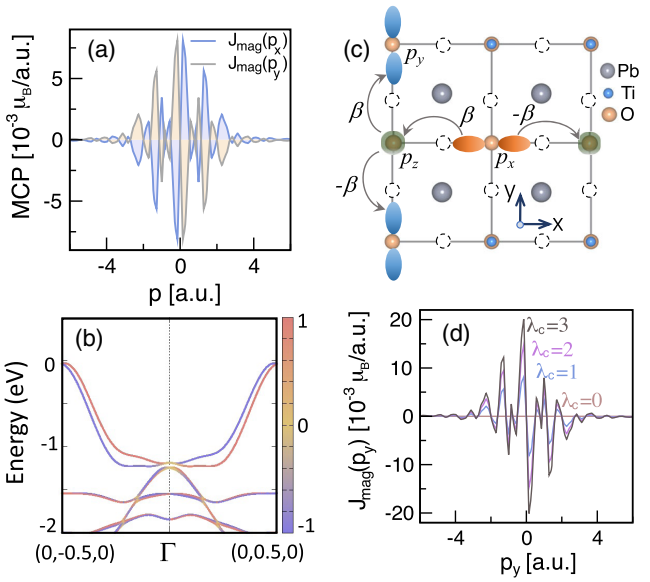

FIG. 2. (a) Calculated MCPs of $PbTiO_3$ along the p_x and p_y directions in momentum space. (b) Band structure of $PbTiO_3$ along $\pm k_y$, showing spin asymmetry (color map) in the S_x spin component. The top of the valence band is set to 0 eV. (c) Illustration of the antisymmetric hopping $\pm\beta$ between O p_x-p_z and p_y-p_z orbitals along $\pm\hat{x}$ and $\pm\hat{y}$ directions respectively, induced by broken $\mathcal{I}$ symmetry. Only hoppings between apical O atoms are indicated. In-plane O atoms are shown in dashed circles. (d) Dependence of the MCP on the enforced SOI strength $\lambda = \lambda_c \times \lambda_r$, with λ_r and λ_c the actual SOI strength and the scaling factor, respectively.

structures are consistent with the presence of $\mathcal{T}$ symmetry, which dictates that the $\uparrow$-spin band at $+\vec{k}$ has the same energy as the $\downarrow$-spin band at $-\vec{k}$, that is $\varepsilon_n(\vec{k}\uparrow) = \varepsilon_n(-\vec{k}\downarrow)$.

Since the spin asymmetry that leads to the MCP is largest at the top of the valence bands, which are predominantly of O-p character, we next analyze the role of the O p orbitals in the chemical bonding, by analyzing the hopping parameters β between neighboring O p orbitals along the $\hat{x}$ and $\hat{y}$ directions. We note that the off-centering of the atoms in the noncentrosymmetric ferroelectric structure induces additional interorbital hoppings between the p_x-p_z and p_y-p_z orbitals of the O atoms, which are forbidden in the Slater-Koster [52,53] parameters in the presence of $\mathcal{I}$ symmetry [see Fig. 2(c)]. Interestingly, the computed effective hopping parameters for the broken symmetry structure [54], have left-right asymmetry [Fig. 2(c)]. Such antisymmetric hopping parameters lead to sine terms in the tight-binding (TB) model, in contrast to the usual cosine terms associated with symmetric hopping, e.g., $\langle p_x | \mathcal{H}_A | p_z \rangle = -2i\beta \sin(k_x a)$. In the small k limit, $\sin(k_x a) \to k_x a$, and the corresponding p-orbital TB Hamiltonian is $\mathcal{H}_A(k) = \gamma(k_x \hat{L}_y - k_y \hat{L}_x)$, where the constant $\gamma \propto \beta$ is a measure of $\mathcal{I}$ asymmetry and $\hat{L}_x, \hat{L}_y$ are the Cartesian components of the orbital angular momentum operator for the p orbitals [55]. We recognize that

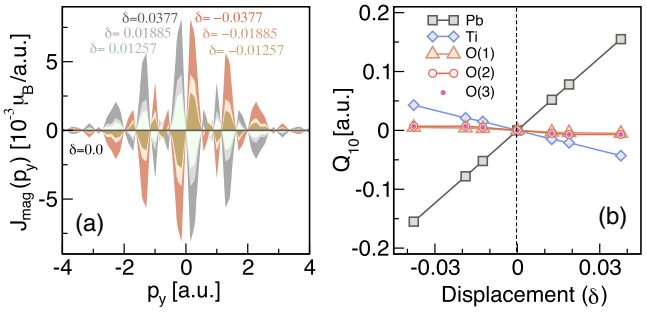

FIG. 3. (a) Variation of MCP with displacement δ (in units of lattice vector c) of the Ti atom from the centrosymmetric position in $PbTiO_3$. The MCP increases with δ, and switches sign as the sign of δ changes. (b) Variation of the odd-parity charge multipole Q_{10} at Pb, Ti, and O sites [apical O(1) and in-plane O(2) and O(3)] for the same displacements δ as in (a). The correlation between Q_{10} and MCP is apparent. The vertical dashed line corresponds to the centrosymmetric case with $\delta = 0$, at which both multipoles and MCP vanish. The odd-parity multipoles at Pb and Ti sites are obtained by adding the p-d and p-s contributions, while for the O atoms only the p-s contribution is considered.

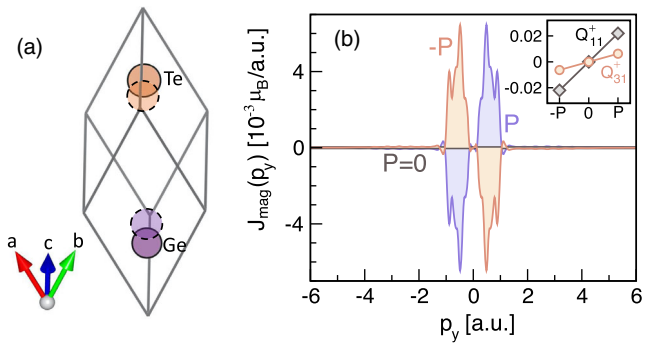

FIG. 4. Switching of MCP in GeTe. (a) The rhombohedral unit cell of GeTe. The dashed atoms indicate the centrosymmetric Ge (0.25,0.25,0.25) and Te (0.75,0.75,0.75) positions; the solid atoms the positions with polarization P. (b) Calculated MCP for structures with polarization P, $-P$, and 0 (for which the MCP vanishes). Inset: odd-parity multipoles Q^+_{11} and Q^+_{31} (in a.u.), which contribute to $J_{mag}(p_y)$, for the antisymmetric spin density with spin quantization along [001]. Multipoles at Ge and Te have opposite sign. Q^+_{11} is summed from its p-d and p-s contributions; Q^+_{31} has only p-d contribution.

$\mathcal{H}_A$ represents the orbital part of the toroidal moment $\mathbf{t}^{(k)}_z$, indicating the crucial role of the antisymmetric hopping between the O p orbitals in generating the k-space toroidal moment.

Since the MCP does not probe the orbital moment of an electron due to the short time spent by the photon probing the electron distribution [56,57], and because the TB Hamiltonian $\mathcal{H}_A(k)$ without including the SOI represents only the orbital part of the toroidal moment, the MCP should vanish in this case. The spin component of $\mathbf{t}^{(k)}_z$, however, appears when the orbitals couple to the spins mediated via SOI, indicating SOI as a crucial ingredient for the MCP. To verify this, we next artificially change the strength of the coupling λ in our calculations. As seen from Fig. 2(d), this results in a drastic change in the magnitude of the MCP, with vanishing MCP at $\lambda = 0$, confirming the importance of SOI.

We now turn to the tuning of the MCP by manipulating the k-space MEMs through changing the real-space odd-parity charge multipoles. We achieve this by scaling the ferroelectric atomic displacements in $PbTiO_3$ along the [001] polarization direction. The resulting changes in MCP are depicted in Fig. 3(a). We also evaluate the corresponding variation in the charge multipoles at the Pb, Ti, and the three O atoms, shown in Fig. 3(b). As expected, the electric dipole at the Pb atom dominates due to the $6s^2$ lone pair that causes the broken $\mathcal{I}$ symmetry. The magnitudes of the dipoles at the Ti and O atoms are rather weak and have the opposite sign to that of the Pb atom. It is also apparent from Figs. 3(a) and 3(b) that the MCP follows the trend in odd parity multipoles: The magnitudes of both increase with increasing ferroelectric displacement and both reverse sign as the displacement is switched. Since the switching of ferroelectric displacements in $PbTiO_3$ can be achieved using an external electric field, our results show the possibility of switching the MCP using electrical means, which may be of practical importance in reducing the experimental uncertainties in a measurement of the effect.

To emphasize the correlation between MCP and odd-parity multipoles, we briefly touch upon the example of ferroelectric GeTe, with electric polarization along the [111] direction of the rhombohedral unit cell [Fig. 4(a)]. The ferroelectric distortion of GeTe [58,59] allows the $\mathbf{t}^{(k)}_x$, $\mathbf{t}^{(k)}_y$ components of the k-space toroidal moment, as well as quadrupole moment components $\mathcal{Q}^{(k)}_{xy}$, $\mathcal{Q}^{(k)}_{yz}$, $\mathcal{Q}^{(k)}_{xz}$, and $\mathcal{Q}^{(k)}_{x^2-y^2}$, in addition to $\mathbf{t}^{(k)}_z$ [see Table I], and the corresponding MCP has more components than in the case of $PbTiO_3$. First, in contrast to $PbTiO_3$, the MCPs in GeTe have simultaneous contributions from toroidal and quadrupole moments rather than pure toroidal contribution. For example, $\{\mathbf{t}^{(k)}_x, \mathcal{Q}^{(k)}_{yz}\}$ contribute to the MCP along p_y with [001] spin quantization axis. Second, even along the same momentum direction, the MCP can appear for different spin quantization axes. For example, along the p_y direction in momentum space, an MCP exists for $\hat{x}$, $\hat{y}$, and $\hat{z}$ spin quantization axes. Knowledge of the odd-parity multipoles is invaluable in interpreting such a complex MCP, and despite the complexity the MCP can again be switched by reversing the direction of polarization [see Fig. 4(b)]. While the magnitude of the MCP is slightly smaller than that of $PbTiO_3$, in GeTe MCP components with parallel spin and momentum directions [e.g., along $\hat{x}$ and $\hat{y}$ driven by $\mathcal{Q}_{x^2-y^2}$ (see Table I)] exist, allowing for experimental detection within the simple backscattering geometry.

Finally, we discuss the proposed experimental setup for detecting the MCP in $PbTiO_3$. The experiment is similar to conventional magnetic Compton scattering, with a circularly polarized beam [60,61], except that an electric field instead of a magnetic field is used to produce a single ferroelectric domain of $PbTiO_3$. The antisymmetric spin profile is obtained either by reversing the circular polarization of the incoming photon and subtracting the two signals, as in the case of conventional magnetic Compton measurements or, more conveniently, by flipping the electric polarization using an electric field at fixed photon helicity. Since electrical switching is much faster than the magnetic-field switching required in a conventional setup, systematic errors due to temporal drifts in photon energy and detector electronics are minimized. Furthermore, systematic errors from imbalance between signal strengths from the two polarization states are eliminated entirely due to the requirement that the difference Compton profile has zero integral. Since the ferroelectric transition temperature for $PbTiO_3$ is $T_c \sim 765$ K [62], the measurements can be done at room temperature.

The k-space MEMs associated with the odd-parity real-space charge multipoles have implications beyond the MCP [63–67]. Examples include a proposed exotic superconducting state driven by odd-parity multipole fluctuations [68,69], and the predicted Rashba effect in $PbTiO_3$ [12], which is a direct consequence of $\mathfrak{t}_z^{(k)}$. Higher order k-space MEMs in $PbTiO_3$ can give rise to a Berry curvature dipole which should lead to a nonlinear Hall effect. Furthermore, the k-space MEMs could conveniently describe the recently observed polar skyrmions [70], in the same spirit as their real-space counterpart forms a basis for describing magnetic skyrmions [18]. We hope that our proposal stimulates experimental efforts to measure the MCP, or these related k-space MEM-driven behaviors, in odd-parity nonmagnetic systems.

We thank Jon Duffy, Stephen Dugdale, and Urs Staub for stimulating discussions. N. A. S. and S. B. were supported by the ERC under the EU's Horizon 2020 research and innovation programme Grant No. 810451 and by the ETH Zurich. Computational resources were provided by ETH Zurich's Euler cluster, and the Swiss National Supercomputing Centre, project ID eth3.

*Corresponding author.
sayantika.bhowal@mat.ethz.ch

[1] S. Datta and B. Das, Appl. Phys. Lett. **56**, 665 (1990).
[2] J. C. R. Sánchez, L. Vila, G. Desfonds, S. Gambarelli, J. P. Attané, J. M. De Teresa, C. Magén, and A. Fert, Nat. Commun. **4**, 2944 (2013).
[3] A. Manchon, H. C. Koo, J. Nitta, S. M. Frolov, and R. A. Duine, Nat. Mater. **14**, 871 (2015).
[4] E. Lesne, Y. Fu, S. Oyarzun, J. C. Rojas-Sánchez, D. C. Vaz, H. Naganuma, G. Sicoli, J. P. Attané, M. Jamet, E. Jacquet, J. M. George, A. Barthélémy, H. Jaffrès, A. Fert, M. Bibes, and L. Vila, Nat. Mater. **15**, 1261 (2016).
[5] S. Manipatruni, D. E. Nikonov, C.-C. Lin, T. A. Gosavi, H. Liu, B. Prasad, Y.-L. Huang, E. Bonturim, R. Ramesh, and I. A. Young, Nature (London) **565**, 35 (2019).
[6] D. Di Sante, P. Barone, R. Bertacco, and S. Picozzi, Adv. Mater. **25**, 509 (2013).
[7] M. Liebmann *et al.*, Adv. Mater. **28**, 560 (2016).
[8] C. Rinaldi, S. Varotto, M. Asa, J. Sławińska, J. Fujii, G. Vinai, S. Cecchi, D. Di Sante, R. Calarco, I. Vobornik, G. Panaccione, S. Picozzi, and R. Bertacco, Nano Lett. **18**, 2751 (2018).
[9] S. D. Stranks and P. Plochocka, Nat. Mater. **17**, 381 (2018).
[10] J. Varignon, J. Santamaria, and M. Bibes, Phys. Rev. Lett. **122**, 116401 (2019).
[11] H. Djani, A. C. Garcia-Castro, W.-Y. Tong, P. Barone, E. Bousquet, S. Picozzi, and P. Ghosez, npj Quantum Mater. **4**, 51 (2019).
[12] R. Arras, J. Gosteau, H. J. Zhao, C. Paillard, Y. Yang, and L. Bellaiche, Phys. Rev. B **100**, 174415 (2019).
[13] C. Ederer and N. A. Spaldin, Phys. Rev. B **76**, 214404 (2007).
[14] N. A. Spaldin, M. Fiebig, and M. Mostovoy, J. Phys. Condens. Matter **20**, 434203 (2008).
[15] N. A. Spaldin, M. Fechner, E. Bousquet, A. Balatsky, and L. Nordström, Phys. Rev. B **88**, 094429 (2013).
[16] H. Schmid, *Introduction to Complex Mediums for Optics and Electromagnetics*, edited by W. S. Weiglhoger and A. Lakhtakia (SPIE Press, Bellingham, WA, 2003), pp. 167–195.
[17] B. B. Van Aken, J.-P. Rivera, H. Schmid, and M. Fiebig, Nature (London) **449**, 702 (2007).
[18] B. Göbel, A. Mook, J. Henk, and I. Mertig, Phys. Rev. B **99**, 060406(R) (2019).
[19] H. Watanabe and Y. Yanase, Phys. Rev. B **98**, 220412(R) (2018).
[20] F. Thöle, A. Keliri, and N. A. Spaldin, J. Appl. Phys. **127**, 213905 (2020).
[21] A. Shekhter and C. M. Varma, Phys. Rev. B **80**, 214501 (2009).
[22] S. W. Lovesey, D. D. Khalyavin, and U. Staub, J. Phys. Condens. Matter **27**, 292201 (2015).
[23] M. Fechner, M. J. A. Fierz, F. Thöle, U. Staub, and N. A. Spaldin, Phys. Rev. B **93**, 174419 (2016).
[24] H. Watanabe and Y. Yanase, Phys. Rev. B **98**, 245129 (2018).
[25] S. Bhowal and N. A. Spaldin, Phys. Rev. Research **3**, 033185 (2021).
[26] R. Nelmes and W. Kuhs, Solid State Commun. **54**, 721 (1985).
[27] N. A. Spaldin, J. Exp. Theor. Phys. **132**, 493 (2021).
[28] The real and momentum space representations are obtained following Ref. [24] and using the compatibility relations [29,30].
[29] T. Inui, Y. Tanabe, and Y. Onodera, *Group Theory and Its Applications in Physics* (Springer, Berlin, 1990), Vol. 78.
[30] J. Perez-Mato, S. Gallego, E. Tasci, L. Elcoro, G. de la Flor, and M. Aroyo, Annu. Rev. Mater. Res. **45**, 217 (2015).
[31] A. H. Compton, Phys. Rev. **21**, 483 (1923).

[32] S. P. Collins, D. Laundy, T. Connolley, G. van der Laan, F. Fabrizi, O. Janssen, M. J. Cooper, H. Ebert, and S. Mankovsky, Acta Crystallogr. Sect. A **72**, 197 (2016).
[33] S. Bhowal, D. O'Neill, M. Fechner, N. Spaldin, U. Staub, J. Duffy, and S. Collins, Open Res. Eur. **1**, 132 (2021).
[34] P. M. Platzman and N. Tzoar, Phys. Rev. B **2**, 3556 (1970).
[35] N. Sakai and K. Ôno, Phys. Rev. Lett. **37**, 351 (1976).
[36] M. J. Cooper, S. P. Collins, S. W. Lovesey, D. Laundy, and D. N. Timms, Phys. Scr. **T35**, 103 (1991).
[37] J. A. Duffy, J. W. Taylor, S. B. Dugdale, C. Shenton-Taylor, M. W. Butchers, S. R. Giblin, M. J. Cooper, Y. Sakurai, and M. Itou, Phys. Rev. B **81**, 134424 (2010).
[38] M. Itou, A. Koizumi, and Y. Sakurai, Appl. Phys. Lett. **102**, 082403 (2013).
[39] E. Zukowski, S. P. Collins, M. J. Cooper, D. N. Timms, F. Itoh, H. Sakurai, H. Kawata, Y. Tanaka, and A. Malinowski, J. Phys. Condens. Matter **5**, 4077 (1993).
[40] J. A. Duffy, J. E. McCarthy, S. B. Dugdale, V. Honkimäki, M. J. Cooper, M. A. Alam, T. Jarlborg, and S. B. Palmer, J. Phys. Condens. Matter **10**, 10391 (1998).
[41] J. A. Duffy, S. B. Dugdale, J. E. McCarthy, M. A. Alam, M. J. Cooper, S. B. Palmer, and T. Jarlborg, Phys. Rev. B **61**, 14331 (2000).
[42] Z. F. Banfield, J. A. Duffy, J. W. Taylor, C. A. Steer, A. Bebb, M. J. Cooper, L. Blaauw, C. Shenton-Taylor, and R. Ruiz-Bustos, J. Phys. Condens. Matter **17**, 5533 (2005).
[43] C. Shenton-Taylor, J. A. Duffy, J. W. Taylor, C. A. Steer, D. N. Timms, M. J. Cooper, and L. V. Blaauw, J. Phys. Condens. Matter **19**, 186208 (2007).
[44] J. A. Duffy, J. Phys. Conf. Ser. **443**, 012011 (2013).
[45] P. E. Mijnarends, S. Kaprzyk, B. Barbiellini, Y. Li, J. F. Mitchell, P. A. Montano, and A. Bansil, Phys. Rev. B **75**, 014428 (2007).
[46] T. Mizoroki, M. Itou, Y. Taguchi, T. Iwazumi, and Y. Sakurai, Appl. Phys. Lett. **98**, 052107 (2011).
[47] B. L. Ahuja, AIP Conf. Proc. **1512**, 26 (2013).
[48] D. Ernsting, D. Billington, T. D. Haynes, T. E. Millichamp, J. W. Taylor, J. A. Duffy, S. R. Giblin, J. K. Dewhurst, and S. B. Dugdale, J. Phys. Condens. Matter **26**, 495501 (2014).
[49] The Elk Code, http://elk.sourceforge.net/.
[50] We used the LDA + SOC formalism and a $6 \times 6 \times 5$ k-point sampling of the Brillouin zone (with no reduction of k-point set, i.e., reducek = 0) to achieve the self-consistency. The MCP is, then, calculated following the implementations, discussed in Ref. [48]. In order to get access to the MCPs along p_y (p_x) for the S_x (S_y) components we rotate the structure about the Cartesian $\hat{y}$ ($\hat{x}$) directions by 90° (270°). The computed MCP is then scaled to the factor that normalizes the valence contribution of the total Compton profile to the total number of valence electrons in the calculation, which is 44 for PTO.
[51] M. A. G. Dixon, J. A. Duffy, S. Gardelis, J. E. McCarthy, M. J. Cooper, S. B. Dugdale, T. Jarlborg, and D. N. Timms, J. Phys. Condens. Matter **10**, 2759 (1998).
[52] J. C. Slater and G. F. Koster, Phys. Rev. **94**, 1498 (1954).
[53] W. A. Harrison, *Electronic Structure and the Properties of Solids: The Physics of the Chemical Bond* (Dover, New York, 1989).
[54] O. K. Andersen and T. Saha-Dasgupta, Phys. Rev. B **62**, R16219 (2000), the effective hopping parameters are extracted using the NMTO downfolding method, described in this reference.
[55] S. Sugano, *Multiplets of Transition-Metal Ions in Crystals* (Academic Press, London, 1970).
[56] D. N. Timms, E. Zukowski, M. J. Cooper, D. Laundy, S. P. Collins, F. Itoh, H. SakuraI, T. Iwazumi, H. Kawata, M. Ito, N. Sakai, and Y. Tanaka, J. Phys. Soc. Jpn. **62**, 1716 (1993).
[57] M. J. Cooper, E. Zukowski, S. P. Collins, D. N. Timms, F. Itoh, and H. Sakurai, J. Phys. Condens. Matter **4**, L399 (1992).
[58] T. Chatterji, S. Rols, and U. D. Wdowik, Front. Phys. **14**, 23601 (2019).
[59] H. L. Kagdada, P. K. Jha, P. Śpiewak, and K. J. Kurzydłowski, Phys. Rev. B **97**, 134105 (2018).
[60] M. Cooper, C. Shenton-Taylor, J. Duffy, C. Steer, and L. Blaauw, Nucl. Instrum. Methods Phys. Res., Sect. A **580**, 1 (2007).
[61] Sensitivity to the MCP arises from a relativistic correction to the scattering cross section (details are given in Ref. [60]). For the ideal case of backscattering, the relative sensitivity to the MCP, compared to the nonmagnetic profile, is reduced by $\sim(2E/m_e c^2)$, where E is the incident photon energy. For 100 keV photons, this amounts to a relatively modest reduction of ~0.4.
[62] G. A. Samara, Ferroelectrics **2**, 277 (1971).
[63] S. Hayami, M. Yatsushiro, Y. Yanagi, and H. Kusunose, Phys. Rev. B **98**, 165110 (2018).
[64] H. Watanabe and Y. Yanase, Phys. Rev. Research **2**, 043081 (2020).
[65] T. Onimaru, K. T. Matsumoto, Y. F. Inoue, K. Umeo, T. Sakakibara, Y. Karaki, M. Kubota, and T. Takabatake, Phys. Rev. Lett. **106**, 177001 (2011).
[66] L. Fu, Phys. Rev. Lett. **115**, 026401 (2015).
[67] M. Yatsushiro and S. Hayami, Phys. Rev. B **102**, 195147 (2020).
[68] J. Ishizuka and Y. Yanase, Phys. Rev. B **98**, 224510 (2018).
[69] S. Sumita and Y. Yanase, Phys. Rev. Research **2**, 033225 (2020).
[70] S. Das *et al.*, Nature (London) **568**, 368 (2019).